Supporting Online Material for

Synchrony Dynamics During Initiation, Failure, and Rescue of the Segmentation Clock

Ingmar H. Riedel-Kruse,* Claudia Müller, Andrew C. Oates*

*To whom correspondence should be addressed. E-mail: ingmar@caltech.edu (I.H.R.-K.), oates@mpi-cbg.de (A.C.O.)

Published 16 August 2007 on *Science* Express
DOI: 10.1126/science.1142538

This PDF file includes:

Supporting online material – Riedel-Kruse et al., 2007

Part A - Materials and methods

1. Fish care and mutant stocks

Zebrafish *Danio rerio* were raised according to standard methods and embryos derived from natural spawning were staged according to (*1*). The allele of the *notch1a* mutant strain *deadly seven* (*des*^{P37A}) was previously described (*2*). For DAPT treatment and microinjection of morpholinos, two parental fish of relevant genotypes were placed in a mesh-bottomed breeding box and allowed to produce embryos for approximately 20-30 min before harvesting. For time series with high temporal resolution, fertilized eggs were removed after 5 min. Embryo clutches were sub-divided into small Petri dishes in groups of 12-20 and incubated at 28.5^{o}C from the 16 cell stage (1.5 hpf) onwards. Clutches with identical developmental progression were subsequently selected, and Petri dishes were fixed with ice cold 4% paraformaldehyde at intervals of 5 min. Given the demonstrated temperature dependence of development in the zebrafish (*1*), extreme care was taken with standardizing handling and growth conditions to achieve reproducible results.

2. DAPT treatment

Embryos were transferred in their chorions into E3 fish media containing varying concentrations of DAPT (*3*), or just 0.1% DMSO carrier, either at hourly intervals throughout development (Fig. 1A,B), or at dome stage (4 hpf) (all other experiments). For rescue or pulse chase experiments, DAPT was washed out by transferring the embryos to fresh E3 + DMSO medium and washing at least 5 times. Embryos were allowed to grow in E3 + 0.03% PTU until 30 - 36 hpf when they were fixed and hybridized with cb1045 riboprobe (*4*) to detect myotome boundaries. Embryos were fixed at intermediate points during the onset of de-synchronization, or rescue of synchronization and hybridized with *dlc* riboprobe.

3. Morpholino design and quantitative injection protocol

Morpholino antisense oligonucleotide (*5*) targeting the 5' UTR of *notch1a* (*6*) was synthesized by Gene-tools LLC (Pilometh, Oregon). Morpholino her1MO3 targeting *her1* has been previously described (*7*), morpholino her1MO4 has the sequence: catggctgaaaatcggaagaagacg. Combined knockdown of *her1* and *her7* was achieved using a total of 0.43 pmol of the previously described her7 MOs (*8*), along with her1MO3 and her1MO4. Part of each injected clutch was grown to 30 hpf and assayed for the complete *her1/her7* somitogenesis phenotype by cb1045 staining.

Morpholino powder was first diluted in sterile Danieau's buffer to 3 mM stock solutions kept at -20^{o}C. Frozen stocks were thawed for 10 min at 65^{o}C, then vortexed and spun down. Concentrations were checked using an Agilent 8453 UV-visible Spectroscopy system at 265 nm in 0.1 N HCl. Working solutions were made from 2 μl MO stock, 2 μl 10x Fast green and 16 μl Danieau's buffer and then further diluted serially in steps 1:1 using 1x Fast green. (1x Fast green = 1ul 10 Fast green+9 μl Danieau's buffer) and stored at +4 ^{o}C. Morpholino working solutions of different concentrations were injected at varying volumes from 0.1 to 1 nL with a Pneumatic

Pico Pump PV 820 (World Precision Instruments) using timed gating, an eject pressure of 40 psi, and applying a back-pressure so as to ensure no liquid in- or out-flux of the needle between injections. Glass needles (Harvard Part No. 30-0020; 1mm O.D.x0.58 I.D.; GC 1000 F-1x) with an opening diameter of ~5 μm were used. The fluid was injected into the yolk center of Zebrafish embryos fertilized not more then 20 minutes earlier, ensuring that resistance from the yolk was uniform between embryos, and hence delivery volume was also regular. Injection into early stages assured full up-take of Morpholino and equal distribution among daughter cells, while injection into later cell stages led to inconsistent results.

For each condition approx. 30 embryos were injected. Before and after injecting a row of embryos, 8 droplets were injected into 15 μl Mineral Oil (Sigma M-3516) that had been placed onto a pre-cleaned (Ethanol, Objective-lens paper (Ross optical lens tissue #5178), final rinse with ddH20) Objective Micrometer (FST No. 29025.02; MA 285; X 1/100 (0.01 mm). The droplets sunk down onto the surface, slightly flattened out, and preserved their shape over tens of minutes. Pictures of these droplets were taken with an Axioscop 2 (Zeiss, Jena), 5x lens at phase-contrast using a Kappa-camera (Supplementary Figure 2). Apparent areas of droplets were measured using Scion Image 1.6 -software, where the area and volume were assumed to scale according to the expected 2/3-power law. This was confirmed with confocal 3-D images of fluorescent droplets of different volumes, finding the geometry preserved (not a sphere due to surface effects). Importantly, the volume depended linearly on the gating time. Independent confirmation of this relationship comes from the observation that varying injection volume and morpholino concentration, but keeping absolute morpholino amount constant, led to consistent ALD phenotypes in the embryo. Morpholino concentrations between 0.125 and 1 mM were tested. Absolute volumes were calibrated using an 80 μm droplet floating in oil. Six droplets before and after injection were each assessed to determine the average and uncertainty in the injected volume. Volumes after injection were typically 5% smaller, indicating partial clogging of the needle. Dramatic differences in the measured volume before and after injection indicated serious experimental problems and were used to exclude a given row of embryos.

We estimated precision and accuracy of our injection protocol to be about 10% each (68% confidence level). All morpholino doses and volumes analyzed were well below the upper limit at which embryos first exhibit necrosis under the head, often accompanied by curvature of the axis, both phenotypes being attributable to non-specific effects due to morpholino toxicity (*9*). After injection, embryos were incubated in E3 at 28^{o}C. After 4-8 hours, embryos that were unfertilized or showed a green blob in the yolk (indicating incomplete morpholino take-up) were removed. Embryos were then transferred into 0.03% PTU (Sigma) to prevent pigment formation, and then incubated at 28.5^{o}C until between 1.5 and 3 dpf. Embryos either self-hatched, or were dechorinated using pronase or by hand, and were then fixed in 4% PFA.

4. In situ hybridization and riboprobe generation

In situ hybridization with *dlc*, *her7* and *her1* riboprobes was performed as described (*7*). The cb1045 probe (*4*) was provided by the Zebrafish International Resource Center (ZIRC; Eugene, Oregon), and was generated by linearizing the pBK-CMV plasmid backbone with SpeI and transcribing with T7 RNA polymerase.

5. Defect scoring

Embryos were visually assessed on a binocular dissection microscope (Olympus SXZ-12). A segment boundary was judged defective when it did not span fully from ventral to dorsal, had a break, or was significantly distorted from its normal shape. Segment boundaries on both sides were scored and the lower value of the two determined the Anterior Limit of Defects (ALD). (Note, that previously (*7, 8*) more conservative measurements have been used, e.g. taking the higher of the two values.) Defects were only scored up to segment 28 and 25 for DAPT and MO experiments, respectively, since later segments are small and were sometimes not well stained. For each data point from the DAPT experiments, between 20-32 embryos were assessed; for the MO experiments, 6 embryos were scored, or in any case where not all of them showed consistent ALDs either below or above 25, 12 embryos were scored. The expectation value for the ALD was then estimated from the median. Scoring by different experimenters was consistent. The Posterior Limit of Defects (PLD) was quantified in an analogous way, but since the number of mis-shaped boundaries cannot be determined with certainty, the position of the vent must be used as a landmark for segment 17. Thus, PLD is currently less reliable than the ALD and represents an estimate.

6. Image analysis

Whole mount embryos were photographed using a Q-Capture Micropublisher on an Olympus SZX12 dissecting microscope using reflected light. Flat mounted tissue was photographed with a Q-Capture Retiga SRV using bright field DIC on a Zeiss Axioskop2 compound microscope. Images were color and contrast balanced in parallel in Adobe Photoshop, then assembled using Photoshop and Illustrator.

7. Data fitting

The data in Fig. 1E,F, and the parameters to eq. 1 were determined with a linear fit using MATLAB (Mathworks Inc.). For Fig. 1F the data points up to t_0 were not included in the fit; the precise position of t_0 was iteratively determined.

The data for the DAPT and the MO experiments in Fig. 2A,B were fitted independently. In both cases all data points from individual embryos were used, instead of the displayed medians at each treatment level. The curves for WT and *des*$^{+/-}$ were fitted together, since the theory predicts a characteristic relation between them (eqs. 7,8). The saturating ALD, $S_{ALD}^{-/-}$, was fixed to the values determined directly from a larger pool of embryos as given in the text and the onset of desynchronization, t_0, was fixed according to the result in Fig. 1F. The parameters R and n_0 were determined by fitting to eq. 7 and using eq. 8. The uncertainty in DAPT concentration was assumed negligible, and the uncertainty in MO dose was inferred from the variation in droplet size. Since fitting in the vicinity of a singularity can lead to substantial artifacts, both data and the fit function were set constant above the maximally scoreable ALD (26 for MO and 29 for DAPT), and a custom-made generalized chi-square fitting routine was used that optimized the chi-square distance along both axes at the same time ("fitChiSquare", MATLAB Central, File Exchange, Mathworks Inc). Uncertainties in the fit parameters were obtained by this routine using Monte Carlo simulations and represent 95% confidence level.

Part B - Mathematical derivations and parameter estimations

The arguments outlined in the main paper contain sufficient information to derive eqs. 6-9 from eqs. 1-5, which allow the organismal phenotype S_{ALD} (=Anterior Limit of Defects, ALD) to be related to the treatment level *n*. Here, we give a more detailed and annotated derivation, to aid the more biologically or theoretically inclined reader on the theoretical or biological aspects, respectively. For excellent and detailed reviews on the segmentation clock and vertebrate somitogenesis, we recommend the reader to (*10-16*).

The parameter estimations stated in the main paper, both for molecular processes and for the critical noise and coupling measurements, are discussed in more detail here as well. Equation numbers with "S" refer to those in this supplement, while those without are found in the main paper.

1. Ansatz equations

The desynchronization hypothesis was put forward by Jiang et al. (*17*), stating that in a Delta or Notch mutant embryo, the coordinated spatiotemporal wave pattern of the genetic oscillators in the PSM breaks down over time, and hence follows a decay process. We test this hypothesis experimentally by reducing the coupling strength among cells and measuring whether the resulting system failure is consistent with a decay of synchrony.

Since neither Notch coupling strength nor synchrony is directly accessible, we seek a theory that relates them to experimentally accessible variables, namely the position of the first defective segment S_{ALD} (ALD) and the treatment level *n* (e.g. the amount of MO delivered to the embryo or the concentration of DAPT the embryo was bathed in).

1.1 Converting real time into segments

The segments are formed under our experimental conditions at a linear rate:

$$\boxed{S = \alpha \cdot t - \mu} \qquad \text{(S1)}$$

with segment number *S*, α=(2.5±0.25)/h and μ=(25±3) (N=6) from our data. This equation is not defined for negative *S*, although negative *S* can be interpreted as oscillations of the system prior to the first segment boundary. This relation converts real time of the decay process into the position of a defective segment in a fixed embryo. Scoring large numbers of fixed embryos is currently much more feasible than a live recording of the segmentation process including its failure.

Note that this constant segment formation rate is not in full agreement with a popular proposal about different rates in anterior vs. posterior segment formation (*1*), but is consistent with measurements made in other labs (*18, 19*).

1.2 Synchrony dynamics of coupled phase oscillators in the presence of noise

Many of the arguments summarized in this section can be followed in more detail in (*20*) p. 283ff. This book discusses synchronization phenomena both with and

without mathematical details, making it useful for a broad audience as well as the mathematically skilled specialist.

We abstract the network of coupled oscillators in the segmentation clock to neglect all spatial aspects of the spatiotemporal wave patterns, how these oscillators are pairwise coupled specifially, and what the oscillation amplitude of each oscillator is. Instead, we use the simplest model possible, where each oscillator is just represented by its oscillation phase and is equally coupled to all other oscillators. In such a case, each oscillator experiences the average influence (or "mean field") of all other oscillators. This representation is similar to the related Kuramoto model for frequency coupling (*21-23*).

This strong abstraction of the segmentation clock is justified since it is among the simplest approaches that can be taken to describe the synchrony dynamics of a large number of oscillators, and thus should be investigated first before more complex models are developed.

How well can the mean field model, which implies equal coupling among all cells, be justified on biological grounds, given that Delta/Notch signaling is usually considered to be a strictly local interaction between direct neighbors? There are several reasons to regard the abstraction as well justified biologically:

Firstly, considering the 3-D packing of spheres, each sphere has on average 12 nearest neighbors; hence, we would expect on average a similar number of neighbors for the coupled cells of the PSM and tailbud.

Secondly, as shown in De Joussineau et al., (*24*) signaling cells extend Delta-containing filopodia and contact cells several diameters away while mediating lateral inhibition in Drosophila. Indeed, we have observed similar cellular processes on Delta-expressing cells in the PSM and tailbud in zebrafish (Supplementary Figure 3). Thus the statement "strictly local" is biochemically true, but the true extent of a cell's locality must be considered in determining to how many other cells a given cell could couple.

These two points therefore suggest that each cells receives input from a few tens of cells, compared to a 1-D chain (e.g. (*25*)), where only two nearest neighbors exist. The mean-field description then would capture the dynamics within every (arbitrarily chosen) patch of cells spanning a distance significantly less than the spatial scales of the wave pattern occurring in the PSM (where the wavelength is tens of cells long). This is actually important, since the phases within these patches are very similar, particularly in the tailbud, making the mean-field different from zero. In contrast, the mean-field over a full wavelength is impractical, since it is zero at all times.

Combined, these arguments let one speculatively estimate that over any chosen volume of approximately 100 cells these mean-field conditions might hold. Since the cells of interest must continue oscillating despite the continual formation of somites in which the oscillations have arrested, such a population ought to be mainly located in the posterior of the tailbud where a persistent tail "stem cell" population has been identified in chick (*26-29*) and mouse (*30-33*).

Finally, an argument is given further down in eq. S6 describing how the notion of synchrony, in the sense that all oscillators have the same phase, can be mathematically generalized to any spatially coordinated phase relation among oscillators, for example, the traveling waves of gene expression with anteriorly shortening wavelength observed in the PSM (*34, 35*). This argument shows that even taking those spatial patterns into account would lead to the essentially the same relation between ALD and treatment level.

If a large number of such phase oscillators are weakly coupled in the presence of noise, the time evolution of the phase Ψ_k of the k^{th} oscillator can be approximated as

$$\frac{d\Psi_k(t)}{dt} = \frac{\varepsilon}{N}\sum_{j=1}^{N}\sin(\Psi_j(t) - \Psi_k(t)) + \xi_k(t) \qquad \text{(S2)}$$

where ε is the pair-wise coupling strength, N is the number of oscillators, t is time, and ξ_k is the white noise that each oscillator experiences, e.g.

$$\langle \xi_k(t) \rangle = 0 \text{ and } \langle \xi_k(t) \cdot \xi_j(t') \rangle = 2\sigma^2\delta_{kj}\delta(t - t'). \qquad \text{(S3)}$$

Here, these oscillators are described in the rotating reference frame, i.e. the average phase has been subtracted from the phases of all individual oscillators. The sine function implies that coupling is acting to decrease phase differences between oscillators, and where this forcing is stronger the larger the phase difference (at least within the phase difference interval from -π/2 to π/2). Noise, on the other hand, leads to random fluctuations in the phase, having a destructive effect on the synchrony among these oscillators.

Synchrony among these oscillators can be quantified by its mean field

$$Z = \frac{1}{N}\sum_{k=1}^{N} e^{i\Psi_k} \qquad \text{(S4)}$$

which is a complex number

$$Z = |Z| \cdot e^{i\varphi} \qquad \text{(S5)}$$

Here the magnitude $|Z|$ denotes the amount of synchronization and φ the average phase of the oscillators. Without loss of generality this average φ can be set to zero and constant in time.

One can generalize the definition of this parameter Z such that it measures whether oscillators have any arbitrary but prespecified phase relation with each other:

$$Z = \frac{1}{N}\sum_{k=1}^{N} e^{i(\Psi_k - \varphi_k)} \qquad \text{(S6)}$$

where the φ_k determines the desired phase relation. For example, consider a linear chain of oscillators with index *k* denoting the oscillators' position in this chain. If one wishes to describe whether these oscillators are coordinated, i.e. synchronized, in a spatially periodic pattern, this phase relation then would be

$$\varphi_k = 2\pi \cdot k / \lambda \qquad \text{(S7)}$$

with λ being the spatial period. If the oscillators are completely synchronized in this specific pattern, Z equals 1 according eq. S6, while according to eq. S4 it would be zero (if averaged over full spatial periods). Hence, the derivations that follow are not limited to homogenously oscillating pattern, but instead generalize to any complex spatial oscillation pattern, and in particular to the traveling waves with anteriorly shortening wavelengths in the PSM (*34*, *35*)

The time evolution of *Z* then is given by

$$\frac{dZ}{dt} = \left(\frac{\varepsilon}{2} - \sigma^2\right) \cdot Z - \frac{\varepsilon^2}{8\sigma^2} \cdot |Z|^2 \cdot Z \qquad \text{(S8)}$$

In the steady state case this leads to a synchronization level given by

$$|Z|^2 = \left(\varepsilon - 2\sigma^2\right) \cdot \frac{4\sigma^2}{\varepsilon^2} \qquad \text{(S9)}$$

Hence, a critical interaction strength $\varepsilon_c = 2\sigma^2$ exists, below which the stable steady state synchrony is zero, i.e. any initial amount of synchrony will decay away. Above this, Z=0 becomes an unstable solution and stability is exchanged onto the upper arm of the bifurcation (Fig. 4H, top), that is, the system will approach a steady state with Z>0.

Neglecting the third order term in eq. S8, $|Z|^2 \cdot Z$, we approximate the time evolution of Z by an exponential decay or build-up starting from the synchronization state $Z(t_0)$ at t_0

$$\boxed{Z(t) = Z(t_0) \cdot e^{-\lambda \cdot (t - t_0)/2}} \quad \text{(S10)}$$

with the time constant

$$\boxed{\lambda = 2\sigma^2 - \varepsilon} \quad \text{(S11)}$$

This time constant is positive or negative, depending on whether noise or coupling dominates, respectively; and λ=0 marks the critical point at the synchronization phase transition.

Such a transition is associated with strong qualitative changes in the collective behavior of the system, in this case there can be (partial) synchrony vs. no synchrony at all when crossing this transition: For λ>0 the synchrony in the system will always decay to 0, while for λ<0 the amount of synchrony will approach some steady state value. A related example for such a phase transition and a critical point is the melting-freezing transition of water, where slight changes in Temperature around the melting-freezing point change the global behavior of the system from water to ice. Temperature changes that happen far away from this critical point change the system properties only quantitatively and in a steady manner.

In the segmenting embryo, when the synchrony Z has decayed below a threshold value Z_c, neighboring cells no longer express segment-determining genes in a coherent cluster, and proper segment formation fails. This point is conveniently assayed by the misformed segment boundary S_{ALD}. Note, that the threshold value Z_c is generally not exactly at the critical point at the synchronization transition; but if the steady state curve for *Z* is very steep close to this critical point (as depicted in Fig. 4H, top), such an assumption is a good approximation. Strictly speaking, it is not even necessary for our conclusion that these two points are approximately the same, but it simplifies the presentation of the arguments.

1.3 Coupling strength among cells

We assume in simplest approximation that the coupling strength, ε, depends linearly on the amount of activated Notch protein, $\bar{p}$:

$$\boxed{\varepsilon = \beta \cdot \bar{p} + A} \quad \text{(S12)}$$

where β is the coupling strength per unit protein. *A* accounts for other potentially existing pathways (Fig 1C), like Wnt signaling (*36, 37*), or other Notch receptors besides Notch1a (*38*).

While in our experiments MO targets only *notch1a* directly, DAPT would be expected to have an effect on other Notches as well, because it inhibits the gamma-secretase activity of Presenilin, an integral membrane protease necessary for the activating cleavage of Notch receptors (*39*). Therefore we expected, and also found, slight quantitative differences in our results between MO and DAPT treatment.

The receptor number is assumed to depend only on steady state kinetics without any additional feedback regulation. This simplest assumption is justified by the absence of changes in *notch1a* expression in *notch1a*, *deltaD*, and *deltaC* mutants, and *her1* and *her7* MO-injected embryos (*7*, *8*). Jiang et al., (*17*) noted an elevation of *notch1a* mRNA in the *mib* mutant, but it is not clear how many different signaling pathways *mib* affects, so this effect could potentially be due to changes in FGF signaling, for example. Of course, the receptor number should drop each time there is a Delta pulse but be replenished continuously, leading on average to a constant level of protein.

It has been found that the level of cleaved Notch1 intracellular domain cycles in the mouse PSM (*40*, *41*). This would make the picture more complicated, but nevertheless we argue that the essentials are already captured by assuming that cell-cell signaling strength is proportional to the average Notch1a protein level over developmental time scales significantly longer than the period of the segmentation clock. In this respect, the large number of gene-dose sensitive Notch phenotypes, including the initial discovery of the Drosophila *Notch* gene in the heterozygote condition due to the "notched" wing margins, is a clear in vivo reflection of the dependence of signaling strength on Notch receptor number (*42*).

1.4 Reduction of activated Notch protein level

A simple approximation to describe the effect of any inhibitory compound applied with an amount or concentration, *n*, on the activated Notch protein level, $\bar{p}$, is given by a Hill equation:

$$\boxed{\bar{p} = \delta \cdot \bar{p}_0 \cdot \left(1 - \frac{n}{n + n_0}\right)} \qquad \text{(S13)}$$

with $2\delta = [0,1,2]$ the number of *notch1a* alleles for homozygous, heterozygous and WT, respectively, $\bar{p}_0$ the WT level of activated protein, and n_0 the treatment level halving $\bar{p}_0$. Note that n_0 therefore is the treatment level equivalent to the heterozygous mutant state.

Depending on how much is known about the reaction kinetics of the particular compound, this or a more realistic but potentially more complicated relation can be derived from these kinetics. We discuss further below (section 3) that the simplest kinetics for mRNA transcription and translation, and mRNA and protein decay lead exactly to the Hill equation stated here. Given that DAPT affects the activated protein by blocking the Presenilin protease, which in turn can cleave multiple Notch receptors, a Hill equation accounting for cooperative effects might be more appropriate:

$$\bar{p} = \delta \cdot \bar{p}_0 \cdot \left(1 - \frac{n^h}{n^h + n_0^h}\right) \qquad \text{(S14)}$$

where *h* is the cooperativity factor. Thus the inclusion of *h* generalizes eq. 5 to more complex chemistries that could potentially be found with alternative inhibitor molecules.

2. Derivation of equations 6 and 7 from the ansatz

Inserting eqs. 1-5 into each other, in order to eliminate the unknown parameters, leads to eqs. 6 and 7 (including the definitions for $n_{c,\delta}$ and R in eqs. 8,9). Here we follow these transformations explicitly:

Inserting eq. S13 into eq. S12 eliminates the activated protein level, $\bar{p}$:

$$\varepsilon = \delta \cdot \beta \cdot \bar{p}_0 \cdot \left(1 - \frac{n}{n + n_0}\right) + A \tag{S15}$$

$$\varepsilon = \delta \cdot \beta \cdot \bar{p}_0 \cdot \frac{n_0}{n + n_0} + A \tag{S16}$$

To account for how the initial synchrony $Z(t_0)$ decays towards the threshold Z_c, we resolve eq. S10 for the absolute time, *t*:

$$\ln\left[Z(t)/Z(t_0)\right] = -\lambda \cdot \left(t - t_0\right)/2 \tag{S17}$$

$$t = t_0 - 2 \cdot \ln\left[Z(t)/Z(t_0)\right]/\lambda \tag{S18}$$

$$t = t_0 + 2 \cdot \ln\left[Z(t_0)/Z(t)\right]/\lambda \tag{S19}$$

This equation we substitute into eq. S1, thereby eliminating absolute time, *t*:

$$S = \alpha \cdot t_0 + 2 \cdot \alpha \cdot \ln\left[Z(t_0)/Z(t)\right]/\lambda - \mu \tag{S20}$$

Now substituting $Z(t)$ with the threshold Z_c, below which no proper segment boundary formation is possible, leads to the defective segment number, S_{ALD}:

$$S_{ALD} = \alpha \cdot t_0 + 2 \cdot \alpha \cdot \ln\left[Z(t_0)/Z_c\right]/\lambda - \mu \tag{S21}$$

Next we eliminate the decay rate λ by substituting eq. S11:

$$S_{ALD} = \alpha \cdot t_0 + 2 \cdot \alpha \cdot \ln\left[Z(t_0)/Z_c\right]/(2\sigma^2 - \varepsilon) - \mu \tag{S22}$$

Finally we substitute eq. S14 to eliminate the coupling strength, ε:

$$S_{ALD} = \alpha \cdot t_0 + 2 \cdot \alpha \cdot \ln\left[Z(t_0)/Z_c\right]/\left(2\sigma^2 - \delta \cdot \beta \cdot \bar{p}_0 \cdot \frac{n_0}{n + n_0} - A\right) - \mu \tag{S23}$$

Now we rewrite this equation in a number of steps:

$$S_{ALD} = \alpha \cdot t_0 + \frac{2 \cdot \alpha \cdot \ln\left[Z(t_0)/Z_c\right]}{2\sigma^2 - A - \delta \cdot \beta \cdot \bar{p}_0 \cdot \frac{n_0}{n + n_0}} - \mu \tag{S24}$$

$$S_{ALD} = \alpha \cdot t_0 + \frac{2 \cdot \alpha \cdot \ln\left[Z(t_0)/Z_c\right] \cdot (n + n_0)}{[(2\sigma^2 - A) \cdot (n + n_0) - \delta \cdot \beta \cdot \bar{p}_0 \cdot n_0]} - \mu \tag{S25}$$

$$S_{ALD} = \alpha \cdot t_0 + \frac{2 \cdot \alpha \cdot \ln\left[Z(t_0)/Z_c\right]/(2\sigma^2 - A) \cdot (n + n_0)}{n + n_0 - \delta \cdot \beta \cdot \bar{p}_0 \cdot n_0/(2\sigma^2 - A)} - \mu \tag{S26}$$

$$S_{ALD} = \alpha \cdot t_0 + \frac{2 \cdot \alpha \cdot \ln\left[Z(t_0)/Z_c\right]/(2\sigma^2 - A) \cdot (n + n_0)}{n - n_0 \cdot \left[\delta \cdot \beta \bar{p}_0 \cdot /(2\sigma^2 - A) - 1\right]} - \mu \tag{S27}$$

Next we define the critical treatment level, $n_{c,\delta}$:

$$n_{c,\delta} = n_0 \cdot \left[\delta \cdot \beta \cdot \bar{p}_0/(2\sigma^2 - A) - 1\right] \tag{S28}$$

For this particular treatment value the denominator in eq. S27 becomes zero and S_{ALD} becomes infinitely large. This is the critical point discussed above (given the approximation discussed before): Below this critical treatment level, the system never decays below the threshold synchrony Z_c theoretically infinitely many segments can

be formed - above the critical level the synchrony decays, and the rate of decay is greater the further away from this critical point. This equation also motivates the definition of a robustness parameter

$$\boxed{R = \beta \cdot \bar{p}_0 / (2\sigma^2 - A) = \varepsilon_{WT} / (2\sigma^2 - A)} \qquad \text{(S29)}$$

which quantifies the contribution of Notch coupling to the robustness (*43*) of the system's synchrony against fluctuations in Notch coupling, other coupling pathways, and noise; a three-way balance that quantifies, for instance, the fold reduction in Notch signaling that is tolerable. For $R>1$ the system has no defects, for $R<0$ the Notch pathway is not required since the other pathways denoted by A are already fully compensating the noise, and for $0<R<1$ the system shows defects. For $R>1$ this value can be interpreted as the answer to: "How many fold can Notch signaling be reduced without resulting in a segmentation phenotype?" Hence $R=2$ indicates that the system is just robust enough such that loss of one allele, i.e., the heterozygous condition, does not show any defect. Note, that this is strictly true only if infinitely many segments would be formed. Given the finite number of somites, it would be tolerable for the system if the synchrony decays over developmental time while Z_c is only crossed after formation of the last segment. Hence the boundary of $R=1$ is an idealization.

This last equation corresponds to eq. 9. Using this definition for R in eq. S28 leads to eq. 8:

$$n_{c,\delta} = n_0 \cdot \left[\delta \cdot R - 1\right] \qquad \text{(S30)}$$

With this definition eq.S27 then reads:

$$S_{ALD} = \alpha \cdot t_0 + \frac{2 \cdot \alpha \cdot \ln\left[Z(t_0)/Z_c\right]/(2\sigma^2 - A) \cdot (n + n_0)}{n - n_{c,\delta}} - \mu \qquad \text{(S31)}$$

Next we write everything with one common denominator:

$$S_{ALD} = \frac{(\alpha \cdot t_0 - \mu) \cdot (n - n_{c,\delta}) + 2 \cdot \alpha \cdot \ln\left[Z(t_0)/Z_c\right]/(2\sigma^2 - A) \cdot (n + n_0)}{n - n_{c,\delta}} \qquad \text{(S32)}$$

In order to utilize the experimentally known ALD for the homozygous mutant, $S_{ALD}^{-/-}$, which is equivalent to a complete knockdown, or any saturating treatment level, we derive the limit of infinitely large treatment level, i.e., $n \to \infty$:

$$S_{ALD}^{-/-} = \lim_{n\to\infty}\left\{\frac{(\alpha \cdot t_0 - \mu) \cdot (n - n_{c,\delta}) + 2 \cdot \alpha \cdot \ln\left[Z(t_0)/Z_c\right]/(2\sigma^2 - A) \cdot (n + n_0)}{n - n_{c,\delta}}\right\} \qquad \text{(S33)}$$

$$S_{ALD}^{-/-} = \lim_{n\to\infty}\left\{\frac{n}{n} \cdot \frac{(\alpha \cdot t_0 - \mu) \cdot (1 - n_{c,\delta}/n) + 2 \cdot \alpha \cdot \ln\left[Z(t_0)/Z_c\right]/(2\sigma^2 - A) \cdot (1 + n_0/n)}{1 - n_{c,\delta}/n}\right\} \qquad \text{(S34)}$$

which simplifies to

$$S_{ALD}^{-/-} = \lim_{n\to\infty}\left\{(\alpha \cdot t_0 - \mu) + 2 \cdot \alpha \cdot \ln\left[Z(t_0)/Z_c\right]/(2\sigma^2 - A)\right\} \qquad \text{(S35)}$$

since $\lim_{n\to\infty}\left\{n_{c,\delta}/n\right\} = 0$ and $\lim_{n\to\infty}\left\{n_0/n\right\} = 0$.

Hence eq. S35 is independent of n, and we find the desired relation:

$$\boxed{S_{ALD}^{-/-} = (\alpha \cdot t_0 - \mu) + 2 \cdot \alpha \cdot \ln\left[Z(t_0)/Z_c\right]/(2\sigma^2 - A)} \qquad \text{(S36)}$$

This is eq. 6. (Setting $\delta=0$ in eq. S27 would have lead to the same relation.)

Rewriting this equation into

$$2 \cdot \alpha \cdot \ln\left[Z(t_0) / Z_c \right] / (2\sigma^2 - A) = S_{ALD}^{-/-} - (\alpha \cdot t_0 - \mu) \quad \text{(S37)}$$

it can now be used to simplify eq. S32 further by substituting the right-hand side:

$$S_{ALD} = \frac{(\alpha \cdot t_0 - \mu) \cdot (n - n_{c,\delta}) + \left[S_{ALD}^{-/-} - (\alpha \cdot t_0 - \mu) \right] \cdot (n + n_0)}{n - n_{c,\delta}} \quad \text{(S38)}$$

Reordering the terms leads to:

$$S_{ALD} = \frac{(\alpha \cdot t_0 - \mu) \cdot n - (\alpha \cdot t_0 - \mu) \cdot n_{c,\delta} + \left[S_{ALD}^{-/-} - (\alpha \cdot t_0 - \mu) \right] \cdot n + \left[S_{ALD}^{-/-} - (\alpha \cdot t_0 - \mu) \right] \cdot n_0}{n - n_{c,\delta}} \quad \text{(S39)}$$

$$S_{ALD} = \frac{S_{ALD}^{-/-} \cdot n + S_{ALD}^{-/-} \cdot n_0 - (\alpha \cdot t_0 - \mu) \cdot n_0 - (\alpha \cdot t_0 - \mu) \cdot n_{c,\delta}}{n - n_{c,\delta}} \quad \text{(S40)}$$

$$\boxed{S_{ALD} = \frac{S_{ALD}^{-/-} \cdot (n + n_0) - (\alpha \cdot t_0 - \mu) \cdot (n_{c,\delta} + n_0)}{n - n_{c,\delta}}} \quad \text{(S41)}$$

This is eq. 7. It is only defined for $n > n_{c,\delta}$, since otherwise the synchrony does not decay below Z_c, and no defective segments are possible.

3. Functional Notch1a protein level and MO injection

notch1a mRNA does not oscillate in zebrafish (*44*), hence we can reasonably assume that it is produced and decays at a constant rate, leading to a stationary level of Notch protein in the absence of Delta signal. The Delta signal depletes this pool of Notch protein in an oscillatory fashion, thereby generating the oscillatory signal (*40, 41*). The amplitude of Notch protein oscillations would depend on whether there is much more Delta than Notch, or visa versa.

The kinetics for mRNA production, decay and binding to MO can be described by

$$\frac{dm}{dt} = a \cdot \delta - k_d \cdot m - K_b \cdot C_{MO} \cdot m \quad \text{(S42)}$$

with m being the amount of mRNA; a, k_d, K_b being the corresponding production, decay and binding rates, and C_{MO} being the MO concentration inside the cell. Since we assume that the MO is evenly distributed among all cells, we find the relation between C_{MO} and the total amount of MO, n, in units of "mol", which was injected into the embryo:

$$C_{MO} = n / V_{cell} / N_{cells} = n / V_{tissue} \quad \text{(S43)}$$

with V_{cell} being the volume of a single cell and N_{cells} being the total number of cells of the embryo at this stage.

Hence in eq. (S42) we can identify an effective mRNA decay-rate:

$$\hat{k}_d = k_d + K_b \cdot C_{MO} \quad \text{(S44)}$$

which can be rewritten as

$$\hat{k}_d = k_d + K_b \cdot n / V_{tissue} \quad \text{(S45)}$$

Therefore, MO-injection can be seen as a tool to remove translatable mRNA from the cell, analogous to an increase in mRNA decay, which suggests it as a powerful tool for quantitative analysis (theoretical and experimental) of genetic networks in general.

This relatively high-throughput strategy can be contrasted to the modification of Hes7 protein stability using knock-in mice (*45*), a much more labor intensive approach leading to a single intermediate phenotype. Of course, the work by Hirata and colleagues (*45*) nevertheless makes a critical contribution - protein and mRNA stability are independent parameters and both likely play roles in determining the dynamics of such a complex genetic system.

Analogous to eq. (S42) the kinetics of protein production and decay are given by:

$$\frac{dp}{dt} = b \cdot m - c \cdot p \tag{S46}$$

with *b*, *c* being the corresponding production and decay rates. In the steady case both eqs. S42, S46 can be set to zero, and then substituted such that mRNA amount *m* is eliminated. This leads to the (steady-state) number of Notch1a receptor given:

$$\bar{p} = \frac{b}{c} \cdot \frac{a \cdot \delta}{\hat{k}_d} = \frac{b}{c} \cdot \frac{a \cdot \delta}{k_d + K_b \cdot n / V_{tissue}} \tag{S47}$$

where δ as before denotes the number of *notch1a* alleles. Rewriting this equation

$$\bar{p} = \frac{a \cdot b}{c \cdot k_d} \cdot \frac{\delta \cdot k_d / K_b \cdot V_{tissue}}{n + k_d / K_b \cdot V_{tissue}} \tag{S48}$$

and redefining variables

$$\bar{p}_0 = \frac{a \cdot b}{c \cdot k_d} \tag{S49}$$

$$n_0 = k_d / K_b \cdot V_{tissue} \tag{S50}$$

which are the WT Notch1a protein amount, and the treatment level halving this amount, respectively, then leads to:

$$\bar{p} = \bar{p}_0 \cdot \frac{\delta \cdot n_0}{n + n_0} \tag{S51}$$

The last equation can be reformulated

$$\bar{p} = \bar{p}_0 \cdot \delta \cdot \frac{n_0}{n + n_0} \tag{S52}$$

$$\bar{p} = \bar{p}_0 \cdot \delta \cdot \frac{n_0 + n - n}{n + n_0} \tag{S53}$$

$$\bar{p} = \bar{p}_0 \cdot \delta \cdot \left(1 - \frac{n}{n + n_0} \right) \tag{S54}$$

This is the Hill equation S13. Thus, eq. 5 of the main manuscript is a good approximation derived from kinetic considerations of the effect of MO binding to mRNA and consequently the amount of functional Notch1a protein.

4. Estimating parameters from the mean-field model and data fitting

Combining our experimental results with theoretical considerations, a number of significant parameters can be estimated. We distinguish here between determining the free parameters in the mean field theory, which is relatively straightforward, and using these parameters to constrain other relations describing the underlying microscopic or molecular properties of the system. These estimations serve as additional tests as to whether the proposed theoretical picture is also justifiable from a

quantitative point of view. Furthermore, many of those parameters have not been estimated or measured before. We first derive the collective properties, noise and coupling of the zebrafish segmentation clock, then estimate the microscopic parameters describing some of the underlying molecular events.

4.1 Noise level, $2\sigma^2$, from macroscopic homozygous *notch1* ALD phenotype:

From eq. 6 we find:

$$S^{-/-} - (\alpha \cdot t_0 - \mu) = 2 \cdot \alpha \cdot \ln\left[Z(t_0) / Z_c \right] / (2\sigma^2 - A) \quad \text{(S55)}$$

$$(2\sigma^2 - A) = \frac{2 \cdot \alpha \cdot \ln\left[Z(t_0) / Z_c \right]}{S^{-/-} - (\alpha \cdot t_0 - \mu)} \quad \text{(S56)}$$

$$2\sigma^2 = \frac{2 \cdot \alpha \cdot \ln\left[Z(t_0) / Z_c \right]}{S^{-/-} - \alpha \cdot t_0 + \mu} + A \quad \text{(S57)}$$

The absolute state of synchronization *Z* is difficult to estimate (both $Z(t_0)$ and Z_c), but only the logarithm of their ratio is of importance. This ratio is always somewhere in the order of unity, since a 3 fold or 100 fold decrease in *Z*, leads to

$$\ln\left(\left| \frac{Z(t_0)}{Z_c} \right| \right) \approx (2.5 \pm 1) \quad \text{(S58)}$$

Furthermore, we set A=0, which means that we estimate the effective noise level with respect to Notch signaling only. More generally, a higher noise might exist, but is already partially countered by other signaling pathways. This higher noise is expected to still be in the same order of magnitude as estimated here.

From the values given in the main paper we estimate the noise to be in the order of:

$$2\sigma^2 = \frac{2 \cdot 2.5 \cdot 2.5 / h}{6 - 2.5 / h \cdot 6h + 25} \approx 0.8/\text{h} \quad \text{(S59)}$$

We therefore conclude that the noise sources combined should be in the order of $2\sigma^2 \approx 0.8$/h to account for the observed ALD in zebrafish mutants encoding components of the Delta/Notch intercellular signaling pathway.

4.2 Noise level from microscopic contributions

In this section we discuss how the total noise level can be related to its individual sources, and how the individual sources can be estimated to an order of magnitude from measurements described in the literature.

4.2.1 Cell movement as noise source:

It has been described (*17*) that in WT embryos, neighboring cells moved relative to each other:

$$x_0 = (2.8 \pm 1.2)\mu m \quad \text{(S60)}$$

as mean and STD over a time of t=10 minutes. More than 50 cells were scored in each of four individual embryos (4.48, 2.43, 1.53, 2.80 μm) – see supplementary information in (*17*) for more detail.

Assuming that these cells undergo a random walk concerning their relative positions we use the definition for the spatial diffusion constant:

$$D_x = x_0^2 / (2dt) \quad \text{(S61)}$$

Here *d* is the dimensionality of the system, and since in (*17*) cells were tracked in the imaging plane, we assume *d*=2. This spatial diffusion constant can be converted into a phase-diffusion constant given the spatial wavelength λ of cyclic gene expression pattern

$$D_\varphi = D_x \cdot \left(\frac{2\pi}{\lambda}\right)^2 \quad \text{(S62)}$$

which in turn then can be related to the noise (*20*)

$$2\sigma^2 = D_\varphi \quad \text{(S63)}$$

This leads to the final relation for the noise due to relative cell movement:

$$2\sigma_{move}^2 = D_\varphi = D_x \cdot \left(\frac{2\pi}{\lambda}\right)^2 = \frac{x_0^2}{4t} \cdot \left(\frac{2\pi}{\lambda}\right)^2 = \pi^2 \left(\frac{x_0}{\lambda}\right)^2 / t \quad \text{(S64)}$$

Assuming the typical length scale of the pattern, i.e. wavelength, of λ=100 μm we find

$$2\sigma_{move}^2 = \pi^2 \left(\frac{x_0}{\lambda}\right)^2 / t = \pi^2 \cdot \left(\frac{2.8\,\mu m}{100\,\mu m}\right)^2 / 10 / \min = 0.05 / h \quad \text{(S65)}$$

This is about an order of magnitude lower than the noise estimated from the homozygous *notch1a* mutant, hence cell mixing via relative movement ought to have a minor contribution to the overall noise, see eq. (S59).

4.2.2 Noise of the individual genetic oscillator

The noise of the individual oscillator can be estimated from (*34*). While observing isolated mouse PSM cells in culture, a period ± STD was found of

$$T=(155\pm34) \text{ min} \quad \text{(S66)}$$

(Published values are ± SEM; STD is personal communication by Ryoichiro Kageyama).

Assuming that ratio between mean and STD is the same in zebrafish, we find for zebrafish with the period of about 30 min

$$T \pm \Delta T=(30\pm6.5) \text{ min} \quad \text{(S67)}$$

The phase diffusion after one cycle then is

$$\Delta\varphi = 2\pi \cdot \frac{\Delta T}{T} \quad \text{(S68)}$$

which corresponds to a phase diffusion constant of

$$D_\varphi = \left(2\pi \frac{\Delta T}{T}\right)^2 / (2T) \quad \text{(S69)}$$

The genetic noise level of an individual cell then is

$$2\sigma_{gen}^2 = D_\varphi = 2\pi^2 \cdot \frac{(\Delta T)^2}{T^3} = 2\pi^2 \cdot \frac{6.5^2}{30^3} / \min = 1.9 / h \quad \text{(S70)}$$

This is about a factor of two higher than the value obtained from the homozygous *notch1a* mutant, see eq. (S59), hence in agreement as an order of magnitude estimation. The true value for this genetic noise of the individual oscillator could well be lower since in those experiments cells have been isolated and therefore likely faced more harsh and noisy conditions than within their natural environment.

4.2.3 Total noise level from microscopic estimations

As mentioned in the main text, there might be additional noise sources than the two discussed and estimated here. In general, these noises add up linearly, i.e.

$$2\sigma_{tot}^2 = 2\sigma_{move}^2 + 2\sigma_{gen}^2 \quad \text{(S71)}$$

For the estimations of these two noise sources we found that noise from cell movement might be rather small compared to the genetic noise of the individual oscillator. This second contribution could already fully account for the noise required to explain the ALD of the *notch1a* embryo phenotype. How well these estimations correspond to the true noise values needs to be shown by future experiments more specifically aiming to determine these parameters.

In conclusion, these noise estimations based on the microscopic behavior of the individual oscillating cells could well account for the noise level that we have deduced from the macroscopic *notch1a* embryo phenotype.

4.3 Coupling strength, ε:

The Notch coupling strength in WT can be directly inferred from the definition of *R* (eq. S29) and the total noise as determined above (eq. (S59)):

$$\varepsilon_{WT} = R \cdot 2\sigma^2 \approx 5 \cdot 0.8 / h \approx 4/\text{h} \quad \text{(S72)}$$

4.4 mRNA-MO binding rate, K_b:

Binding rates between MO and mRNA have not been measured directly to our knowledge. Since MO has the same bases as DNA it is reasonable to use binding rates found among polynucleotides in general. We assume that MO effectively binds irreversibly to mRNA in a concentration dependent way, supported by the fact that mRNA can be stabilized by MO in the embryo (*7, 47*), and by in vitro measurements (*48*). In this study of mRNA binding to short DNA strands, a biphasic binding was observed, e.g. a slow and a fast binding rate constant (*48*). These phases typically differed by 2-3 orders of magnitude, hence in first approximation one phase could be neglected. These *in vitro* rates for mRNAs between 17 and 37 nucleotides ranged from $(10^4 - 10^6) / M / s \approx 10^5 / M / s$, with the general trend that shorter strands had higher rates. Since commercially available MOs have 25 nucleotides, and given a slower diffusion inside a cell, we assume that the in vivo mRNA-MO binding rate is at the lower end of the measured range, that is:

$$K_b = \sim 10^4/\text{M/s} \quad \text{(S73)}$$

In general, the values for such a mRNA-MO binding rate for different genes may span some orders of magnitudes, very likely due to differing energies of secondary structure disruption, as well the GC content (see examples from (*48*) above). In that respect it has also been found that two MOs against different target regions of the same mRNA are often required to achieve a strong mRNA knockdown (*49*), which suggests that one MO opens up the secondary structure for the second MO to bind reliably.

4.5 The endogenous *notch1a* mRNA decay rate:

According to eq. S50

$$k_d = K_b \cdot n_0 / V_{tissue} \quad \text{(S74)}$$

we can directly estimate the *notch1a* mRNA decay rate, where n_0 is determined by the fit in Fig. 2B, V_{tissue} can be estimated, which is presumably similar to the

unfertilized egg with diameter d = 600 μm, $V_{tissue} = \pi \cdot d^3 / 6 \approx 0.1$ μl; K_b is used us estimated before, leading to

$$k_d \approx 10^4 / M / s \cdot 0.02 \cdot 10^{-12} mol / (0.1 \cdot 10^{-6} / l) \approx 0.1 / \min \quad \text{(S75)}$$

The decay of *her7* mRNA has been estimated at 0.24/min, consistent with the cyclic behavior of this gene (*46*). The slightly higher rate for *notch1a* estimated here would imply that it takes the mRNA longer than a cycle to decay, but that it would decay over the time corresponding to a small number of cycles. For instance, when the segmentation clock has finished its task in the late-stage embryo, *notch1a* mRNA would become absent. Hence this estimated mRNA decays rate is of reasonable magnitude, supporting the estimate of the in vivo mRNA-MO binding rate.

4.6 Conclusions

Using the data obtained from quantitative knock-down of gene function with either MOs or small molecule inhibitors, we were able to deduce several parameters essential for the description of the system's dynamics. Although the uncertainties in some of these parameters are rather large, they are likely of the right order of magnitude. A less abstract description than the mean-field, perhaps taking all the spatio-temporal details into account, would also require a pair-wise interaction strength similar to that proposed here, but probably not differing more than a factor of ~3. Furthermore, these estimations demonstrate how future experiments aimed at specific parameters (such as decay rates or binding constants) improve precision for other parameters, like the relationship between the in vivo MO-mRNA binding rate and the natural mRNA decay rate, which are directly related.

Supplementary figure 1

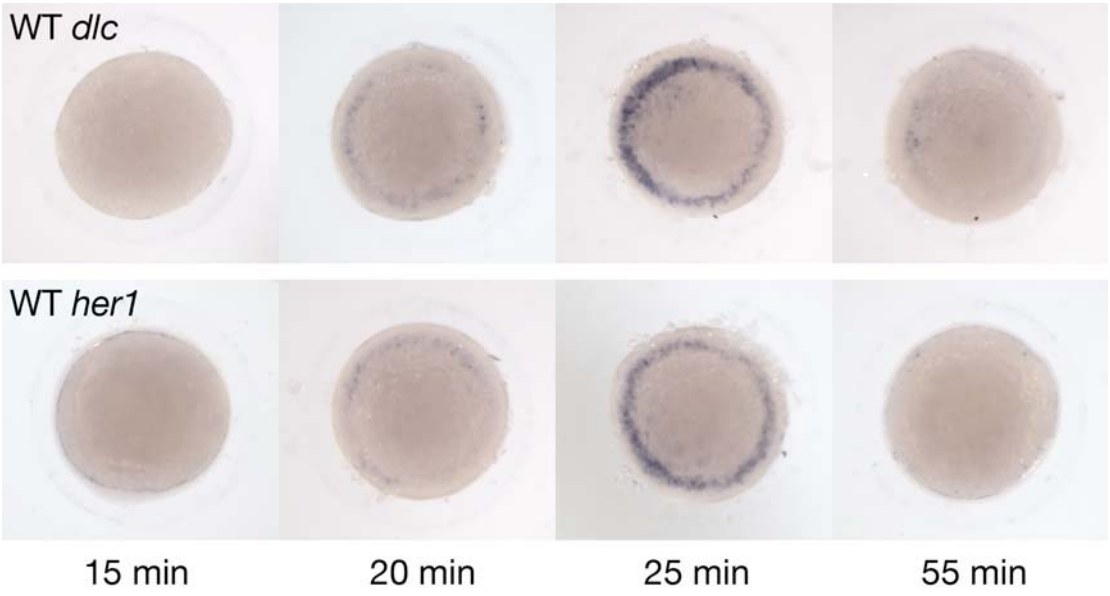

Supplementary Figure 1. Onset of cyclic *dlc* and *her1* expression in the blastula. Animal pole views of embryos staged with 5 min time intervals from 30 % to the onset of gastrulation hybridized with riboprobes to *dlc* (upper panels) or *her1* (lower panels). Times given under the panels refer to the developmental stages shown in Figure 3B and C. Note the rapid and simultaneous onset of gene expression seen in the presumptive mesoderm of the blastula margin from 15 to 25 min, and the almost total loss of expression in these cells 30 min later.

Supplementary figure 2

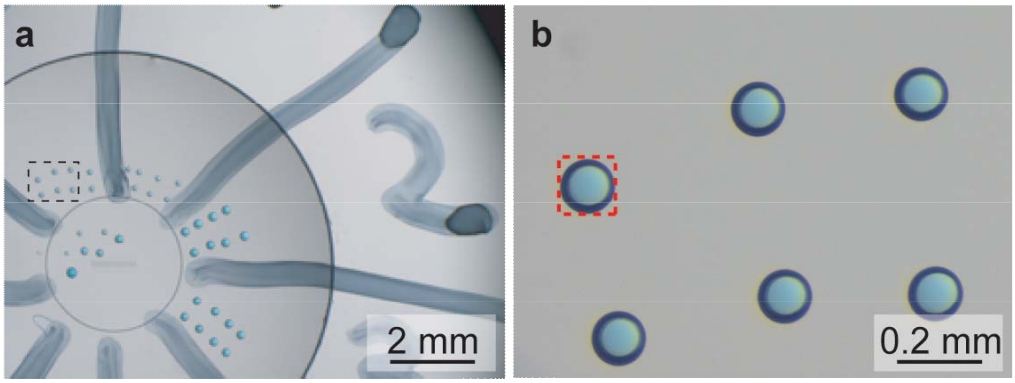

Supplementary Figure 2. Measurement of MO droplet volumes.
a. Overview of a stage micrometer test slide, showing the clusters of injection droplets in oil sitting in regions corresponding to a particular row of embryos (for example, row 2). The micrometer used for initial drop size calibration (length =1 mm) is in the center of the smaller circle. b. Higher magnification view of the droplets boxed in (a), showing six used for quantification.

Supplementary figure 3

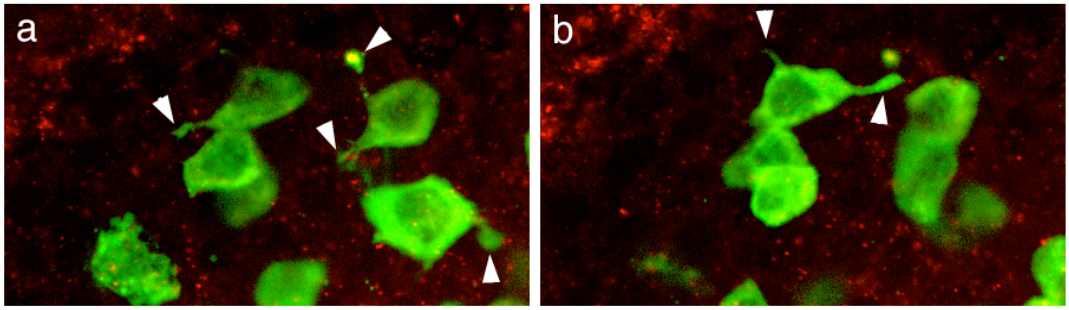

Supplementary Figure 3. Extended cellular processes in the tailbud.
Confocal images of fluorescently labeled, transplanted cells (green) in the tailbud of non-labeled host embryos (red = *notch5* transcript). Cell bodies are approximately 10 μm in diameter, and multiple cellular processes are extended by cells for comparable distances (arrowheads). (a) and (b) are 2 separate 1 μm thick optical planes, spaced 6 μm apart. Experimental details given in (*50*).

References

1. C. B. Kimmel, W. W. Ballard, S. R. Kimmel, B. Ullmann, T. F. Schilling, *Dev Dyn* **203**, 253 (1995).
2. F. J. van Eeden *et al.*, *Development* **123**, 153 (1996).
3. A. Geling, H. Steiner, M. Willem, L. Bally-Cuif, C. Haass, *EMBO Rep* **3**, 688 (2002).
4. M. Deniziak *et al.*, *Exp Cell Res* **313**, 156 (2007).
5. A. Nasevicius, S. C. Ekker, *Nat Genet* **26**, 216 (2000).
6. S. A. Holley, D. Julich, G. J. Rauch, R. Geisler, C. Nusslein-Volhard, *Development* **129**, 1175 (2002).
7. A. C. Oates, R. K. Ho, *Development* **129**, 2929 (2002).
8. A. C. Oates, C. Mueller, R. K. Ho, *Dev Biol* **280**, 133 (2005).
9. S. C. Ekker, J. D. Larson, *Genesis* **30**, 89 (2001).
10. A. Aulehla, B. G. Herrmann, *Genes Dev* **18**, 2060 (2004).
11. J. Dubrulle, O. Pourquie, *Development* **131**, 5783 (2004).
12. F. Giudicelli, J. Lewis, *Curr Opin Genet Dev* **14**, 407 (2004).
13. S. A. Holley, *Genes Dev* **20**, 1831 (2006).
14. S. A. Holley, C. Nusslein-Volhard, *Curr Top Dev Biol* **47**, 247 (2000).
15. O. Pourquie, *Science* **301**, 328 (2003).
16. P. C. Rida, N. Le Minh, Y. J. Jiang, *Dev Biol* **265**, 2 (2004).
17. Y. J. Jiang *et al.*, *Nature* **408**, 475 (2000).
18. E. Hanneman, M. Westerfield, *J Comp Neurol* **284**, 350 (1989).
19. K. Schmidt, J. M. Starck, *J Exp Zoolog B Mol Dev Evol* **302**, 446 (2004).
20. A. Pikovsky, M. Rosenblum, J. Kurths, *Synchronization - A universal concept in nonlinear sciences*, Cambridge Nonlinear Science Series (Cambridge University Press, Cambridge, UK, 2003).
21. Y. Kuramoto, in *International symposium on mathematical problems in theoretical physics* H. Araki, Ed. (Springer Verlag, 1975), vol. 39, pp. 420-422.
22. Y. Kuramoto, *Chemical oscillations, waves, and turbulence* (Springer Verlag, Berlin, 1984).
23. S. H. Strogatz, *Physica D* **143**, 1 (2000).
24. C. De Joussineau *et al.*, *Nature* **426**, 555 (2003).
25. K. Horikawa, K. Ishimatsu, E. Yoshimoto, S. Kondo, H. Takeda, *Nature* **441**, 719 (2006).
26. G. C. Schoenwolf, V. Garcia-Martinez, M. S. Dias, *Dev Dyn* **193**, 235 (1992).
27. Y. Hatada, C. D. Stern, *Development* **120**, 2879 (1994).
28. D. Psychoyos, C. D. Stern, *Development* **122**, 1523 (1996).
29. M. A. Selleck, C. D. Stern, *Development* **112**, 615 (1991).
30. S. Eloy-Trinquet, L. Mathis, J. F. Nicolas, *Curr Top Dev Biol* **47**, 33 (2000).
31. S. Eloy-Trinquet, J. F. Nicolas, *Development* **129**, 3609 (2002).
32. J. F. Nicolas, L. Mathis, C. Bonnerot, W. Saurin, *Development* **122**, 2933 (1996).
33. V. Wilson, R. S. Beddington, *Mech Dev* **55**, 79 (1996).
34. Y. Masamizu *et al.*, *Proc Natl Acad Sci U S A* **103**, 1313 (2006).
35. I. Palmeirim, D. Henrique, D. Ish-Horowicz, O. Pourquie, *Cell* **91**, 639 (1997).
36. A. Aulehla *et al.*, *Dev Cell* **4**, 395 (2003).
37. M. L. Dequeant *et al.*, *Science* **314**, 1595 (2006).

38. J. Westin, M. Lardelli, *Dev. Genes Evol.* **207**, 51 (1997).
39. Y. Morohashi *et al.*, *J Biol Chem* **281**, 14670 (2006).
40. S. S. Huppert, M. X. Ilagan, B. De Strooper, R. Kopan, *Dev Cell* **8**, 677 (2005).
41. M. Morimoto, Y. Takahashi, M. Endo, Y. Saga, *Nature* **435**, 354 (2005).
42. S. Artavanis-Tsakonas, M. D. Rand, R. J. Lake, *Science* **284**, 770 (1999).
43. N. Barkai, S. Leibler, *Nature* **387**, 855 (1997).
44. C. Bierkamp, J. A. Campos-Ortega, *Mech Dev* **43**, 87 (1993).
45. H. Hirata *et al.*, *Nat Genet* **36**, 750 (2004).
46. J. Lewis, *Curr Biol* **13**, 1398 (2003).
47. M. Gajewski *et al.*, *Development* **130**, 4269 (2003).
48. P. Schwille, F. Oehlenschlager, N. G. Walter, Biochemistry 35, 10182 (1996).
49. B. W. Draper, P. A. Morcos, C. B. Kimmel, Genesis 30, 154 (2001).
50. A. C. Oates, L. A. Rohde, R. K. Ho, Dev Biol 283, 204 (2005).